Strojniški vestnik - Journal of Mechanical Engineering 52(2006)3, 161-169
UDK - UDC 621.952:539.37
Izvirni znanstveni članek - Original scientific paper (1.01)

Analiza deformacij vrtal po analitični metodi in s končnimi elementi

Deformation Analysis of Boring Bars Using Analytical and Finite Element Approaches

Ahmet Taşkesen[1] - Faruk Mendi[1] - Yasin Kisioglu[2] - Mustafa Kemal Kulekci[3]
([1]Gazi University, Ankara; [2]The Ohio State University, Columbus Ohio; [3]Mersin University, Tarsus)

V prispevku obravnavamo analizo deformacij vrtal z uporabo analitične metode in metode končnih elementov. Izbrali smo tri vrste krožnih vrtal iz hitro reznega jekla in cementno-karbidnimi lastnostmi, za katera smo z uporabo obeh metod izračunali deformacije, nastale pod vplivom posrednih vrtalnih sil. Predlagali smo priporočilo izdelovalcem, s katerim lahko določijo obseg napak, ki vplivajo na odstopanje izmer in natančnost končne obdelave površine lukenj, izvrtanih vrtali, ki se upognejo zaradi vrtalnih sil. Ugotovili smo tudi, da stožčasta vrtala niso primerne oblike za vrtanje dolgih lukenj.

(Ključne besede: procesi vrtanja, analize deformacij, metode končnih elementov)

In this paper we discuss the deformation analyses of boring bars using analytical and finite-element methods. Three types of circular boring bars with HSS and cemented-carbide properties were selected, and their deformations when subjected to oblique boring forces were calculated using both methods. A guideline is proposed for the manufacturer, who can determine the extent of the errors that affect the dimensional tolerance and the surface-finish accuracy of the bored hole produced by the bar bent when subjected to the boring forces. Also, we observed that a conical bar is not an appropriate design for boring a long hole.

(Keywords: boring bars, boring processes, deformation analysis, finite element methods)

0 INTRODUCTION

Manufacturers usually select a boring process to achieve the desired dimensional accuracy when dealing with cases of large holes (e.g., diameter > 25mm) as an alternative approach to the conventional drilling and surface finishing [1]. The boring process enlarges holes previously drilled and offers straightness, parallelism, positional accuracy, size control, surface finish, improved accuracy of the dimensions and tolerance, and the elimination of any possible eccentricity. The surface quality of the bored hole, including the desired dimensional accuracy, is dependent on selecting the appropriate boring processes, including depth of cut, cutting speed, and the geometry of the boring bars. When the depth of cut and the elasticity of the material exceeds a certain limit, then the roughness of the surface of the machine components becomes unacceptable and tool breakage can occur. Usually, it is not recommended to have the ratio of the bar length, L, to the bar radius, r_b, i.e., L/r_b, larger than 10 to 12 when using steel or cemented-carbide materials [1]. Rather than using expensive experimental descriptions, the deformation of boring bars with different geometries and materials can be analyzed using both analytical and computer-aided finite-element methods to determine the appropriate shape of the bar for an acceptable process. Permissible stresses for the bars, known as design stresses, are usually low ([8] and [9]). However, the amount of deflection of the boring bar is usually high, so that boring errors occur in the dimensions of the desired hole.

The objective of this paper was to analyze the bar deformations and determine the appropriate bar design using both high-speed-steel (HSS) and cemented-carbide materials for boring bars at the recommended limit ratio (L/r_b) of 12. From the design point of view, bar deflection is one of the most troublesome elements for boring bars. When it exceeds the allowed limit [2], dimensional tolerance errors can occur on the diameter of the bored hole.

1 DEFORMATION ANALYSIS OF THE BORING BAR

Boring bars are usually made in three geometrical shapes: the square shank, the round shank, and the solid-carbide round shank [1]. Round-shank boring tools find wide application in industry, while the other two, because of manufacturing difficulties, have very limited applications. For this reason, in this paper, round-shank boring bars are discussed. The boring process is an oblique metal-cutting process, in which the tool is considered stationary and the workpiece is rotating about its axis [8]. Some of the procedures for dealing with boring-bar deformation analysis are described below.

1.1 Selecting Geometrical Models

Three types of geometrical models selected for boring bars, corresponding to the rules of the manufacturing and design processes, are shown in Figure 1. Each model was selected in accordance with possible geometrical conditions and the mechanical design methodologies. The three selected models shown in the figure have the same length and bar diameter: Model A is a traditional straight bar with a shoulder, but without a fillet. Model B has a variable front-end radius (r) and a constant rear-end radius (r_b), the ratio (r/r_b) of which ranges from 0.5 to 1. And finally, Model C has a shoulder with a large fillet radius, which enables it to be more flexible and resistant to the stress concentration and deformation due to notch effects.

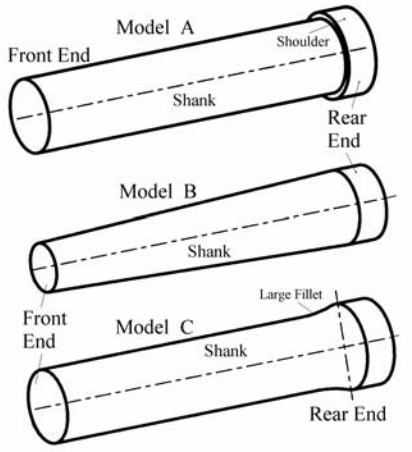

Fig. 1. *Selected circular geometrical models of boring bars*

1.2 Analytical Approach

Our goal is to derive a formulation that accurately describes the shank deformation of the boring bar due to oblique boring forces (OBFs), depending on certain variables such as the depth of cut (chip thickness), cutting edge angle, length and diameter of the bar, geometrical variables, and material properties. Figure 2 shows a boring tool consisting of a boring bar, an inserted cutter tip, and adjustment and set screws. The cutter tip is usually inserted onto the boring bar with an angle of 53°08' [1]. The boring bar can be clamped in any position in the turret (support). With this type of boring tool, the bar can be extended beyond the holder just far enough to reach the length of the hole to be bored, which makes the tool very rigid. In analytical deformation analysis, the values of the specific shear pressure, K_s, of each of the HSS-steel and carbide-steel material couples for the boring process [1] are considered. When we consider a constant cutting speed of 30 m/min for the boring process and the feed per revolution of 0.2 mm, the values of the specific cutting pressures are selected from the appropriate tables [1] as 2000 MPa and 2800 MPa for the HSS-steel and the carbide-steel material couples, respectively. In addition, the depth of cut is selected, ranging from 1 mm to 3 mm. The Young's Modulus is also selected from tables as 200 GPa and 400 GPa for the HSS and carbide materials, respectively [3].

The OBF at the front end of the boring tool creates torsion and bending moments during the

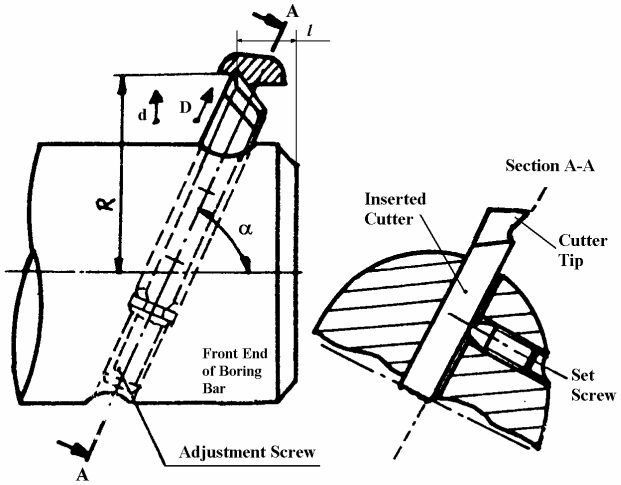

Fig. 2. *The components of a boring tool*

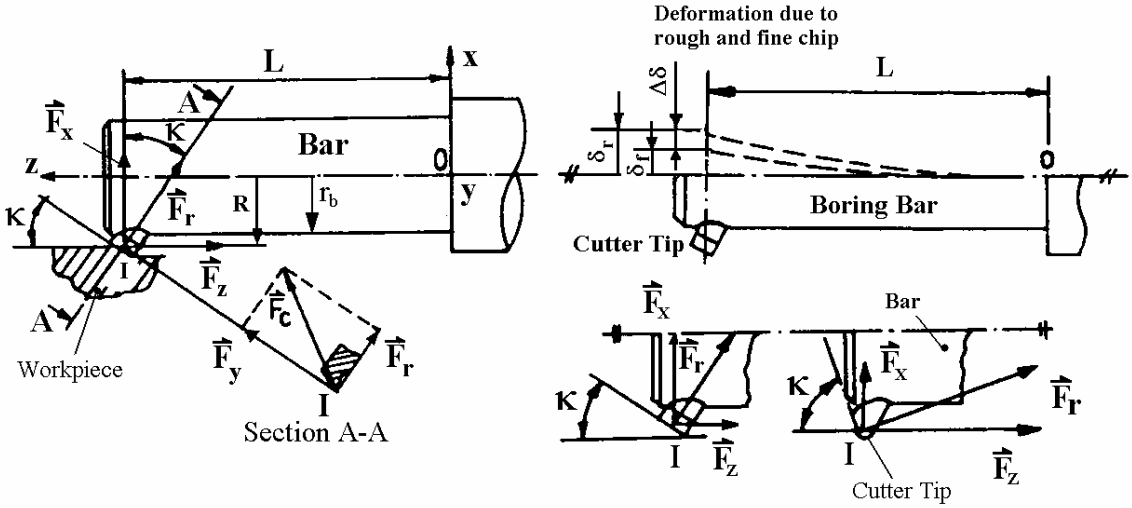

Fig. 3. *Distribution of the OBF and deflection due to the rough- and fine-chip processes*

boring process in such a way that the moments create deflection on the boring bar. A rigid bar subjected to the OBF at the interaction point 'I' of the cutter and workpiece and their resultants are shown in Figure 3. The radial and axial forces in the x-z projection plane have a resultant force, F_r. The distribution of the OBF on a single-point cutting tool is not a constant but depends on the cutting edge angle, κ, as shown in Figure 3. Experiments have shown that if κ is 45°, then the boring forces can be distributed as F_x, F_y, and F_z components, in the ratio 1:5:2 [1]. The three forces, F_x, F_y, and F_z, acting on the boring bar will do the bending, torsion, and compression, respectively. As shown in the equations below, the OBFs depend on the cutting-edge angle, the chip thickness, and the feed per revolution. Indeed, the three components of the OBF, F_x, F_y, and F_z, affect the boring bar through the tip of the cutting tool during the operation process. The tangential, radial, and axial forces within the corresponding directions, respectively, can be found using the following equations:

$$F_y = t_c \cdot s \cdot K_s \tag{1}$$

$$F_x = F_r \cdot \sin\kappa \tag{2}$$

$$F_z = F_r \cdot \cos\kappa \tag{3}.$$

Where: $F_r = 2 \cdot F_y / 3$ when $30^o < \kappa < 70^o$ [1]
$F_r = F_y / 3$ when $70^o < \kappa < 90^o$ [1]
t_c : chip thickness (mm)
s : feed per revolution (mm/rev)
K_s : specific shear pressure of the material (MPa)
κ : cutting edge angle.

1.3 Quantitative Description of the Boring Bar Deformation

The boring bars, considered as a cantilever beam, must be capable of deflection under the OBF. In the case of analytical deflection analysis, the most popular approach, strain energy by Castigliano's theorem, is applied instead of the many other available approaches. The strain energy for a combined, loaded boring bar is a nonlinear function of the OBF and the bending moment [7]. In applying Castigliano's second theorem in this application, the strain energy for a circular boring bar subjected to the OBF, such as the axial forces F_z, pure bending moment $M = F_x \cdot L$, shearing due to bending V, and the torque $T = F_y \cdot r_b$, can be rewritten in terms of the OBF and the bending moments as follows:

$$U = \int \frac{F^2 \cdot dz}{2A \cdot E} + \int \frac{M^2 \cdot dz}{2E \cdot I} + \int \frac{\alpha_s \cdot V^2 \cdot dz}{2A \cdot G} + \int \frac{T^2 \cdot dz}{2J \cdot G} \tag{4}.$$

Generally, the translational (δ_i) and rotational (θ_i) displacements of the boring bar can be performed by partial derivation of the strain-energy equation (4) with respect to the general OBF (F_i) and general torsional couple (T_i), respectively. Therefore, the translational and rotational displacements of the circular boring bar can be obtained using the following convenient form of equations, in the corresponding x, y, and z directions. Here, the integration is carried out over the boring-bar length to calculate the bar deflection in the related directions, i.e.:

$$\delta_x = \left(\frac{\partial U}{\partial F}\right)_z = \int \frac{\alpha \cdot V}{A \cdot G} \cdot \frac{\partial V}{\partial F} \cdot dz + \int \frac{M}{E \cdot I_y} \cdot \frac{\partial M}{\partial F} \cdot dz - \int \frac{M}{E \cdot I_x} \cdot \frac{\partial M}{\partial F} \cdot dz \tag{5}$$

$$\delta_y = \left(\frac{\partial U}{\partial F}\right)_z = \int \frac{\alpha \cdot V}{A \cdot G} \cdot \frac{\partial V}{\partial F} \cdot dz + \int \frac{M}{E \cdot I_y} \cdot \frac{\partial M}{\partial F} \cdot dz + \int \frac{T}{G \cdot J} \cdot \frac{\partial T}{\partial F} \cdot dz \quad (6)$$

$$\delta_z = \left(\frac{\partial U}{\partial F}\right)_z = \int \frac{F_z}{A \cdot E} \cdot \frac{\partial F_z}{\partial F} \cdot dz - \int \frac{M}{E \cdot I_y} \cdot \frac{\partial M}{\partial F} \cdot dz + \int \frac{M}{E \cdot I_x} \cdot \frac{\partial M}{\partial F} \cdot dz \quad (7),$$

by the same token, the rotational displacement (twist angle), δθ, which occurs only about the 'z' axis, can be written as follows:

$$\delta_\theta = \int_0^L \frac{T}{2J \cdot G} \cdot \frac{\partial T}{\partial T} \cdot dz \quad (8),$$

from which the boring-bar deflections in both the translational and rotational directions can be written as follows:

$$\delta_x = \frac{F_x \cdot L}{G \cdot A_2} + \frac{F_x \cdot L^3}{3E \cdot I_x} - \frac{F_z \cdot r_b \cdot L^2}{2E \cdot I_y} \quad (9)$$

$$\delta_y = \frac{F_y \cdot L}{G \cdot A_1} + \frac{F_y \cdot L^3}{3E \cdot I_x} + \frac{F_y \cdot r_b^2 \cdot L}{G \cdot J} \quad (10)$$

$$\delta_z = \frac{F_z \cdot L}{E \cdot A} - \frac{F_x \cdot r_b \cdot L}{3E \cdot I_x} + \frac{F_z \cdot r_b^2 \cdot L}{2E \cdot I_y} \quad (11)$$

$$\delta_\theta = \frac{F_y \cdot r_b \cdot L}{G \cdot J} \quad (12).$$

Where: $\delta_{x,\ y,\ and\ z}$: translational deflections in the direction of the x, y and z-axes,

δθ: rotational deflection about the z-axis,

E: Young's modulus of the boring bar material

G: shear modulus of the boring-bar material

$I_x = I_y = \pi \cdot r_b^4/4$: moment of inertia

$J = \pi \cdot r_b^4/4$: polar moment of inertia

$A = \pi \cdot r_b^2$: cross-sectional area of the boring bar

$A_1 = A_2 \cong 0.9A$: shearing area [1]

α_s: shear form factor.

The resultant deflection of the boring bar in 3-D can be calculated as follows:

$$\delta = \sqrt{\delta_x^2 + \delta_y^2 + \delta_z^2} \quad (13).$$

When changing the condition of the boring process during the operation, the deflection of the boring bar does not remain constant. For instance, in the transition from the rough to the fine chip process during the operation, the bar deflection is variable. This variation, as shown in Figure 3, causes the dimensional tolerance errors in the bored-hole dimensions. Considering the deflection δ_r due to the rough chip and δ_f due to the fine-chip processes, the variation of the deflection can be defined as follows:

$$\Delta\delta = \delta_r - \delta_f \quad (14)$$

From this we can say that Δδ causes the dimensional accuracy of the bored hole, which can be determined in the following equation:

$$D_{bh} = D_{dh} - 2 \cdot \Delta\delta \quad (15),$$

where D_{bh} and D_{dh} are the bored and desired hole diameters, respectively.

As a result, from Equation (15), the D_{bh} would be made much bigger than D_{dh} without dimensional tolerances. For this reason, it is highly recommended to avoid the transition from the rough-chip to the fine-chip process during the boring operations.

1.4 Finite-Element Analysis (FEA) Approach

The bending deflections for all types of boring bars are carried out with FEA using the ANSYS computer-code software. The results from the simulations are compared with the corresponding analytical results for the validation of our boring-bar models.

1.4.1 FEA mesh generation and boundary conditions

It is very important to select the mesh generation that is characterized by a structural solid element to enable us to describe the boring-bar behavior because of the difficulties in dealing with the geometrical model. The structural solid element provides us with information about the degrees of freedom (DOFs) related to the translational and the rotational displacements. Basically, the element is defined by four nodes, each node has six DOFs, i.e., three of them are translational in the x, y, and z directions, the other three are rotational about the x, y, and z-axes [4]. Besides the mesh generation, suitable boundary conditions are applied for each type of every bar model by using these FEA mesh generations, as shown in Figure 4. Considering the conditions of the boring process, the boring bars have free rotational DOFs about the axis of rotation, the z-axis, but all the nodes are restricted to rotations about the x- and y-axes. On the other hand, all other nodes have free translational DOFs in the three axes, except the clamped area at the rear end, and the OBFs are applied at point 'I'.

1.4.2 Deflections of the boring bars

By applying the different amounts of OBF as a function of the chip thickness using Equations (1),

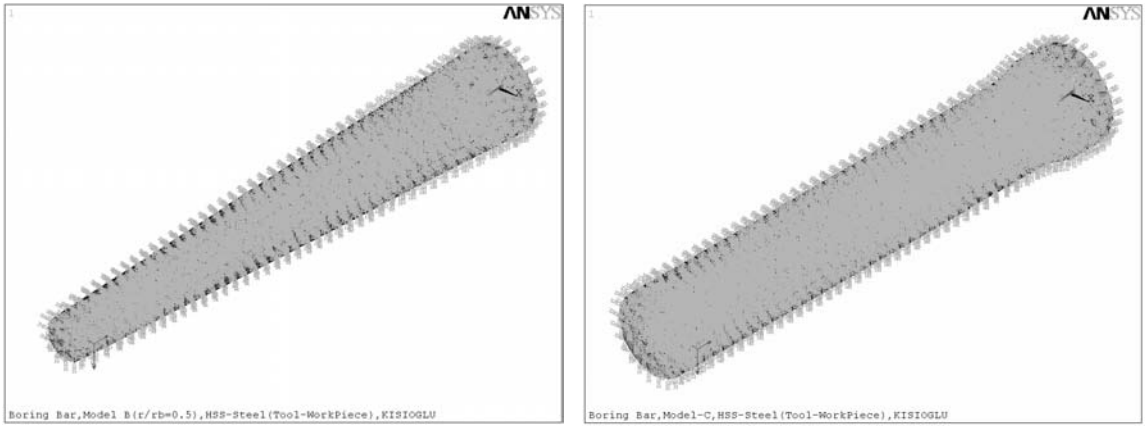

Fig. 4. *FEA mesh generation and boundary conditions for Models B (0.5), and C*

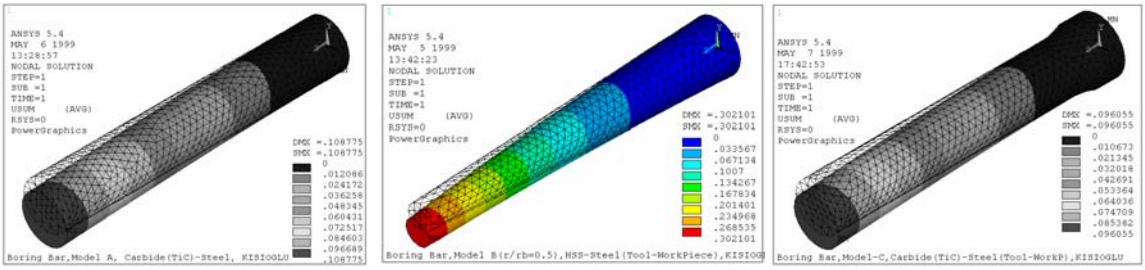

Fig. 5. *Contour plots of the translational deflections for three types of bar Models*

(2) and (3), the FEA models are simulated and some results are obtained. The translational deflections for Models A, B, and C are shown in Figure 5. For all the simulation-pictures, the dashed and solid lines show the undeformed and deformed geometries of the bar, respectively. On the other hand, the rotational deflections of the three models are also obtained. The rotational deflections, however, are very small, and do not cause the manufacturing errors mentioned in the literature as well. For this reason, the rotational deflection of the boring bars is not demonstrated in detail as contour plots from the simulations.

1.4.3 Experimental Investigation

Experiments have been conducted to further examine the validity of the analytical and FE methods. The boring tests were carried out without lubricant. A dynamometer with high sensitivity was set up to measure the cutting forces and the deflections. A specifically designed tool holder mechanically locked in the front of the dynamometer was used to hold the ANSI TPN 431 carbide tools. The cutting conditions were appropriately selected to obtain continuous chip flow. The chip thickness was set to be: 1.2, 1.4, 1.6, 1.8, 2, 2.2, 2.4, 2.6, 2.8, and 3 mm. The cutting speed was chosen as 30 m/min. The data are shown in Table 1.

1.4.4 Data and results

Table 1, below, shows the translational deflection data for all types of boring bars, having properties of the HSS-steel material couples. These values of the deflections are obtained from bending tests under the OBF of the boring bars by applying both the analytical and FEA approaches. The first column shows the depth of cut in mm. In the second column, the magnitude of the bar deflections as a function of depth of cut is given by applying Equation (13) of the analytical approach. The rest of the columns show the translational deformations of all types of boring bars by applying the FEA approach. The numbers in the brackets in columns 3 to 6 show the ratia (r/r_b) of Model B. Likewise, Table 2, below, shows the translational deflection data for all types of boring bars, having the properties of the cemented carbide-steel material couple by applying both analytical and FEA approaches. Figure 6, below, shows the relationship between the translational and rotational deflections for all types of boring bars as

Table 1. Translational deflections of the boring bar using the HSS-steel material couple from both analytical and FEA approaches

Boring Bar Deflection (USUM) Using HSS-Steel Couple Materials						
t_c(mm)	Analyt. Model	Model A & B(1)	Model B (0.5)	Model B (0.67)	Model B (0.83)	Model C
1	0.117751743	0.129492	0.251674	0.182973	0.154614	0.114348
1.2	0.141302092	0.155291	0.302101	0.229481	0.185538	0.137219
1.4	0.164852441	0.181291	0.352589	0.268149	0.216481	0.16009
1.6	0.188402789	0.207194	0.40305	0.306501	0.247391	0.182964
1.8	0.211953138	0.233091	0.4535075	0.344884	0.278725	0.205833
2	0.235503487	0.258988	0.5039691	0.383283	0.309743	0.228701
2.2	0.259053836	0.284903	0.5544307	0.4244896	0.340694	0.251574
2.4	0.282604184	0.310811	0.6048923	0.464093	0.371726	0.274445
2.6	0.306154533	0.336719	0.6553539	0.503696	0.402757	0.297316
2.8	0.329704882	0.362627	0.7058155	0.543299	0.433789	0.320187
3	0.35325523	0.388535	0.7562771	0.582902	0.464821	0.343058

Table 2. Translational deflections of the boring bars with the cemented carbide-steel material couple from both analytical and FEA approaches

Total Deflection (USUM) Using Carbide-Steel Couple Materials						
t_c (mm)	Analyt. Model	Model A & B(1)	Model B (0.5)	Model B (0.67)	Model B (0.83)	Model C
1	0.082617129	0.090646	0.175914	0.133865	0.108231	0.080073
1.2	0.099140555	0.108775	0.211097	0.160638	0.129879	0.096055
1.4	0.115663981	0.12691	0.24665	0.187042	0.151532	0.112069
1.6	0.132187407	0.145034	0.281929	0.214184	0.173171	0.128073
1.8	0.148710833	0.163166	0.317245	0.240962	0.194822	0.144085
2	0.165234259	0.181291	0.352558	0.268127	0.216463	0.16009
2.2	0.181757685	0.1994225	0.3879265	0.2947454	0.238113	0.1760921
2.4	0.198281111	0.2175517	0.4232677	0.3215861	0.259759	0.1920972
2.6	0.214804537	0.2356809	0.4586089	0.3484268	0.2814055	0.2081023
2.8	0.231327962	0.2538101	0.4939502	0.3752675	0.303052	0.2241074
3	0.247851388	0.2719393	0.529291	0.4021081	0.3246985	0.2401125

a function of the depth of cut when using the properties of the HSS-Steel material couple for the boring process. As the figure shows in the first graphics using data from Table 1, the translational deflections of Model C using both the analytical and FEA approaches are consistent. In the second graphics, the rotational deflections for all types of bar models are not consistent. The results from the FEA approaches are obtained higher than the analytical approach. The data for the rotational deflections are obtained using Equation (12) for the analytical approach. The data table of the rotational deflections is not shown here. Similarly, the graphical relationships of the translational and rotational deflections of all types of boring bars are shown in Figure 7 using the data in Table 2, taking into consideration the properties of the cemented carbide-steel material couples for the boring process. As can be seen in the first graphics using the data from Table 2, the translational deflections of Model C using both the analytical and FEA approaches are also consistent. In the second graphics, the rotational deflections for all types of bar models are not consistent. The results from the FEA approaches are found higher than the analytical approach. The data for the rotational deflections are obtained using Equation (12) for the analytical results. The data table of the results is not shown here. Indeed, in general, the rotational displacement is not sufficient to cause the boring errors in the bar, nor is it considered seriously in the related literature. Figure 8, below, illustrates the variation of the bar deflection in both the translational and rotational directions as a function of the ratio r/r_b of Model B. The figure shows a rapid decrease in the bar deformation, whereas 'r' increases, as explained above. The

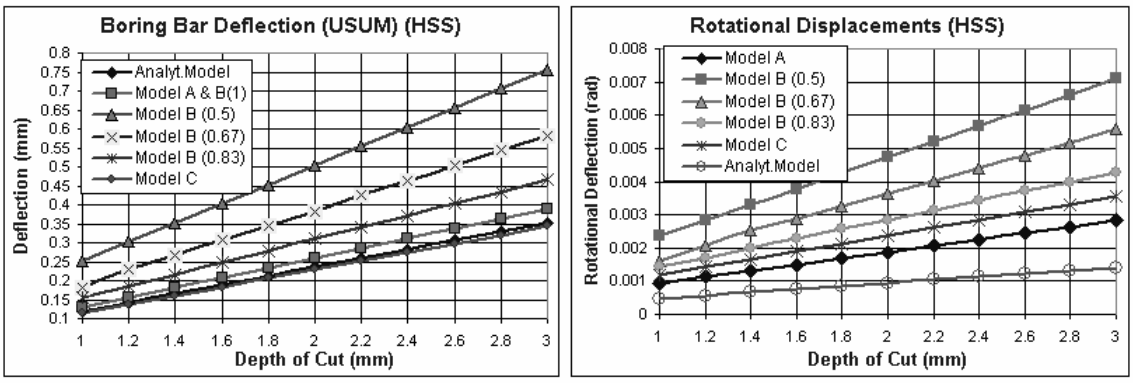

Fig. 6. *Graphical results of bar deflections in translational and rotational directions from both the analytic and the FEA approaches (material: HSS-steel couple)*

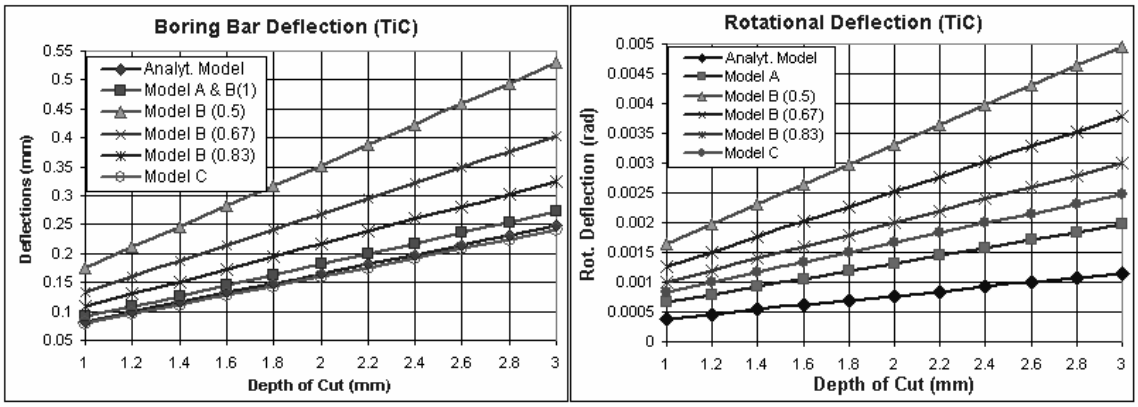

Fig. 7. *Graphical results of bar deflections in translational and rotational directions from both the analytical and the FEA approaches (material: cemented carbide-steel couple)*

variation in the rotational deflection as a function of conical ratio is found to be more than the variation of the translational deflection. The trends of both variations are also different.

1.5 Qualitative Description of Bar Deformation

Considering the deflections in the x, y, and z directions, the δ_z deflection is very small, whereas the δ_x and δ_y are bigger, as mentioned above. In this case, the δ_x and δ_y are especially important. In particular, if the δ_x exceeds the allowable limit, then it causes tolerance errors on the surface finish. However, if the δ_y exceeds the permissible limit, which causes a certain error "*e*", as shown in Figure 9, then the desired size control and the dimensional accuracy of the desired bored hole may not be obtained. Thus, we can find the error '*e*', as given by Equation (16) below. The δ_y will specify the degree of surface roughness. In this situation, '*e*' can be treated as an error and can be calculated using the Pythagorean theorem, knowing that it is related to the size of the bored hole and the deflection, δ_y, in the vertical direction in the case of the analytical model, as is given by Equation (10), above. In other words:

$$e = R - (R^2 - \delta_y^2)^{1/2} \tag{16}$$

where $R = r_b + (l \cdot \tan\alpha)$ (see Figure 1.)

The magnitude of the translational deflection's errors of the boring bars Models A, B (0.83) and C as a function of the depth of cut are shown in Figure 10 when considering the properties of both HSS-steel and cemented-carbide-steel material couples and using both analytical and FEA approaches. Both graphics illustrate that the smallest errors are obtained when Model C, with any type of material properties, is considered as the bar geometry for the boring process. Both solution approaches, the analytical and the FEA analysis, showed that the magnitude of the errors for Model C is consistent with both graphics in Figure 10.

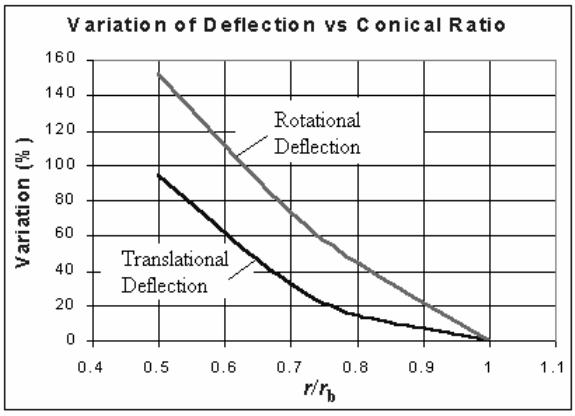

Fig. 8. *The boring bar deformation vs. the conical ratio of Model B*

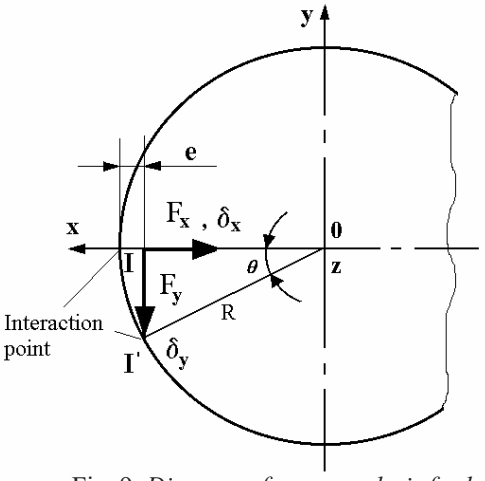

Fig. 9. *Diagram of error analysis for bar deformation*

2 DISCUSSION AND CONCLUSIONS

The deformation of the boring bar is modeled accurately by the driven analytical equations and validated by a computer-code finite-element method. Both the analytical and the FEA approaches confirm that Model C is an appropriate boring-bar design. From Figures 6 and 7 it is clear that the deflections of boring bars for both the analytical and FEA models are increasing with the depth of cut. But generally, the trends are the same. From the figures we can conclude that the twisting angle is very small, and that the rotational deformation is not important in the case of bar-design considerations and a bored hole with the desired characterizations. Figure 8, on the other hand, shows that the deflection is inversely proportional to the conical ratio (r/r_b), so that reducing r increases the deflection. Therefore, using a conical shape in the design of the boring bar is not appropriate for a long hole. On the other hand, the results found for Models A, B (0.83) and C, as shown in Figure 10, may be used by manufacturers as guidelines to determine the boring errors that affect the bored hole's dimensional tolerance and surface-finish accuracy according to the depth of cut.

Finally, the main purpose in the boring process with a boring bar is to reduce the tangential force F_y by making the cutting edge angle κ and the diameter of the bar as large as possible. For the same reason, the length of the bar L must be chosen to be as small as possible. In order to design a boring bar in the form of Model C, certain criteria must be followed. The amount of deformation must be restricted to a certain value and, on the other hand, the vibration must be absorbed and the effects of the notch between the shoulder and the bar must be reduced by a large fillet. Generally, if we change the boring process conditions like the chip thickness, the feet rate, etc. during the operation, the bar deformation becomes variable. This will create dimensional errors in the desired bored hole (size control, surface finish etc.). Indeed, the constant deformation is a special case that leads to dimensional tolerance errors in the size control.

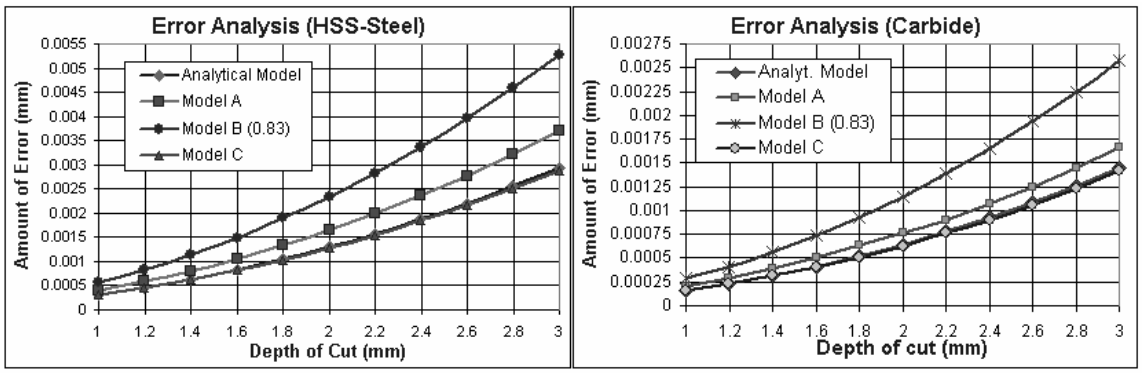

Fig. 10. *The magnitude of the error on the boring-bar deflections*

3 REFERENCES

[1] F. Mendi, T. Tezgahlari (1996) Teori ve Hesaplari, *72 TDFO Ltd. Sti.*, Ankara, Turkey.
[2] S.T. Nagano, T. Koizumi, T. Fujii, N. Tsujiuchi, H. Ueda, and K. Steel (1997) Development of a composite boring bar, *Composite Structures*, 38 (1997) 531-539.
[3] E. A. Avallone, T. Baumeister (1987) Marks' standard handbook for mechanical engineers, *McGraw-Hill Inc*.
[4] ANSYS User Manual (1998) ver. 5.4.
[5] T. Tyan, W.H. Yang (1992) Analysis of orthogonal metal cutting processes, *International Journal for Numerical Methods in Engineering*, 34 (1992) 365-389.
[6] A.J. Shih (1995) Finite element simulation of orthogonal metal cutting, *Journal of Engineering for Industry*, 117(1995) 84-93.
[7] A.C. Ugural, S.K. Fenster (1995) Advanced strength and applied elasticity, *Prentice Hall*.
[8] P.F. Oswald, J. Munoz (1997) Manufacturing processes and systems, *John Wiley & Sons*.
[9] M.C. Shaw (1996) Metal cutting principles, *Oxford University press*.

Authors' Addresses: Dr. Ahmet Taşkesen
Dr. Faruk Mendi
Gazi University
Technical Education Faculty
Besevler, Ankara, 06503
Turkey

Dr. Yasin Kisioglu
The Ohio State University
Industrial, Welding and
Systems Engineering
Columbus Ohio 43210
U.S.A.

Dr. Mustafa Kemal Kulekci
Mersin University
Tarsus Technical Education
Faculty
33480 Tarsus
Turkey
mkkulekci@mersin.edu.tr

Prejeto: 1.6.2005
Received:
Sprejeto: 16.11.2005
Accepted:
Odprto za diskusijo: 1 leto
Open for discussion: 1 year